

Research Paper

Influence of transboundary air pollution on air quality in southwestern China



Xiufeng Yin^{a,b,c}, Shichang Kang^{a,c,d}, Maheswar Rupakheti^e, Benjamin de Foy^f, Ping Li^g, Junhua Yang^a, Kunpeng Wu^h, Qianggong Zhang^{b,d}, Dipesh Rupakheti^{a,*}

^a State Key Laboratory of Cryospheric Science, Northwest Institute of Eco-Environment and Resources, Chinese Academy of Science, Lanzhou 730000, China

^b Key Laboratory of Tibetan Environment Changes and Land Surface Processes, Institute of Tibetan Plateau Research, Chinese Academy of Sciences, Beijing 100101, China

^c University of Chinese Academy of Sciences, Beijing 100039, China

^d CAS Center for Excellence in Tibetan Plateau Earth Sciences, Beijing 100085, China

^e Institute for Advanced Sustainability Studies, Potsdam, Germany

^f Department of Earth and Atmospheric Sciences, Saint Louis University, St. Louis, MO 63108, USA

^g Northwest Institute of Eco-Environment and Resources, Chinese Academy of Science, Lanzhou 730000, China

^h Institute of International Rivers and Eco-Security, Yunnan University, Kunming 650091, China

ARTICLE INFO

Article history:

Received 18 January 2021

Revised 7 May 2021

Accepted 21 May 2021

Available online 24 May 2021

Handling Editor: M. Santosh

Keywords:

Air pollutants

Transboundary transport

Southwestern China

ABSTRACT

Air pollution is a grand challenge of our time due to its multitude of adverse impacts on environment and society, with the scale of impacts more severe in developing countries, including China. Thus, China has initiated and implemented strict air pollution control measures over last several years to reduce impacts of air pollution. Monitoring data from Jan 2015 to Dec 2019 on six criteria air pollutants (SO₂, NO₂, CO, O₃, PM_{2.5}, and PM₁₀) at eight sites in southwestern China were investigated to understand the situation and analyze the impacts of transboundary air pollutants in this region. In terms of seasonal variation, the maximum concentrations of air pollutants at these sites were observed in winter or spring season depending on individual site. For diurnal variation, surface ozone peaked in the afternoon while the other pollutants had a bimodal pattern with peaks in the morning and late afternoon. There was limited transport of domestic emissions of air pollutants in China to these sites. Local emissions enhanced the concentrations of air pollutants during some pollution events. Mostly, the transboundary transport of air pollution from South Asia and Southeast Asia was associated with high concentrations of most air pollutants observed in southwestern China. Since air pollutants can be transported to southwestern China over long distances from the source regions, it is necessary to conduct more research to properly attribute and quantify transboundary transport of air pollutants, which will provide more solid scientific guidance for air pollution management in southwestern China.

© 2021 China University of Geosciences (Beijing) and Peking University. Production and hosting by Elsevier B.V. This is an open access article under the CC BY-NC-ND license (<http://creativecommons.org/licenses/by-nc-nd/4.0/>).

1. Introduction

Air pollutants adversely affect human health, agricultural productivity, the climate system, snow fields and glaciers, and hydrological cycle, and thus they are getting more attention recently (Chan and Yao, 2008; Kan et al., 2012; Guan et al., 2016; Song et al., 2017; Zhang et al., 2017). Emissions of air pollutants from one country can affect countries and ocean basin downwind. Massive outflow of emissions of air pollutants from China has been reported to results in high concentrations of air pollutants downwind, for example over remote islands in Japan (Oki Island and

Okinawa Island) (Murano et al., 2000), during the high-PM₁₀ episode in Seoul, Korea (Oh et al., 2015). Verstraeten et al. (2015) attributed that transport of ozone and its precursors from China has offset about 43% of emissions reduction in free-tropospheric ozone over the western United States that was expected between 2005 and 2010. As the second-largest economy and the largest developing country in the world, China has experienced rapid economic and social development in the past decades and has become one of the largest emitters of air pollutants. However, China also receives regional air pollutants transported from across its boarder. Li et al. (2016) reported, based on the isotopic analysis of carbon ($\delta^{13}\text{C}$), a significant influence of black carbon (BC) from South Asia to the Tibetan Plateau in China. Yin et al. (2018) found that high concentrations of total gaseous mercury observed at the back-

* Corresponding author.

E-mail address: drupakheti2@gmail.com (D. Rupakheti).

ground site in the inland Tibetan Plateau were associated with the air masses transported from South Asia. Kang et al. (2019) reviewed a number of previous studies on the transport of air pollutants from South Asia to the Tibetan Plateau, and concluded that the emissions of various air pollutants, including particulate matter (e.g., Cong et al., 2015; Lüthi et al., 2015; Li et al., 2016; Yang et al., 2019) and gaseous species (e.g., Sheng et al., 2013; Yin et al., 2018) from South Asia can be transported to the Tibetan Plateau crossing the Himalayas.

South Asia and Southeast Asia are densely populated regions with rapidly growing economies and suffer from heavy air pollution (Shi et al., 2018; Saikawa et al., 2019). Southwestern China shares borders with several South Asian and Southeast Asian countries. Air pollutants transported across the border from these neighboring countries to southwestern China is expected to comprise a significant portion of the regionally transported pollutants. In recent decades, China has reduced the sources of air pollutants significantly using measures from both central and local governments (Wang and Hao, 2012; Zhang et al., 2012) and air quality is improving nationwide (Wang et al., 2016; Zhao et al., 2018; Yin et al., 2019). While the domestic emissions are being controlled, transboundary transport of air pollutants to China and its impacts deserve more attention, especially from South Asia and Southeast Asia.

Many previous studies focused on the air quality at sites in eastern China (e.g., Wang et al., 2014; Ma et al., 2016; Zhao et al., 2016). The research on air pollutants in southwestern China is limited, and there are very few studies about transboundary transport of air pollutants to this region of China (Cheng et al., 2019). Yunnan Province (hereinafter Yunnan) is one of the developing provinces in southwestern China, with fewer heavily polluting industries and thus relatively lower emission of air pollutants than those in eastern China. To assess the impact of air pollutants transported across the border from South Asia and Southeast Asia on air quality in

southwestern China, we investigated temporal and spatial characteristics of gaseous and particulate air pollutants observed during 2015–2019 at eight sites in Yunnan located near the border between China and the neighboring countries in South Asia and Southeast Asia. The potential source regions and transboundary transport of air pollutants were analyzed by using the HYSPLIT (HYbrid Single-Particle Lagrangian Integrated Trajectory) model simulations, CWT (Concentration Weighted Trajectory), and available emission inventories. This study utilized for the first time a limited set of ground based observational data from southwestern China and those observations were interpreted using other available data, including outputs of model simulations (flowchart of process and method is shown in Supplementary Data, Fig. S1). The key focus was to document and attribute the transboundary transport of air pollutants in this less-studied region (the southwestern China) so that it would instigate more attention and further research on this serious environmental problem.

2. Materials and methods

2.1. Measurement sites and air pollutants data

In this study, air pollutants monitored during a 5-year period (2015–2019) at eight sites (Shangri-La, Lushui, Baoshan, Mangshi, Lincang, Jinghong, Mengzi, and Wenshan) along the border of Yunnan province in southwestern China with neighboring countries were investigated (Fig. 1). Yunnan is located at the far southeastern edge of the Tibetan Plateau and has a mild climate, and it is influenced by the continental air masses that carry urban/industrial and biomass burning emissions from South Asia and Southeast Asia as well as maritime air masses from both the Pacific Ocean and Indian Ocean. All these urban sites are located in small cities in China, with a population <1 million and the gross domestic product

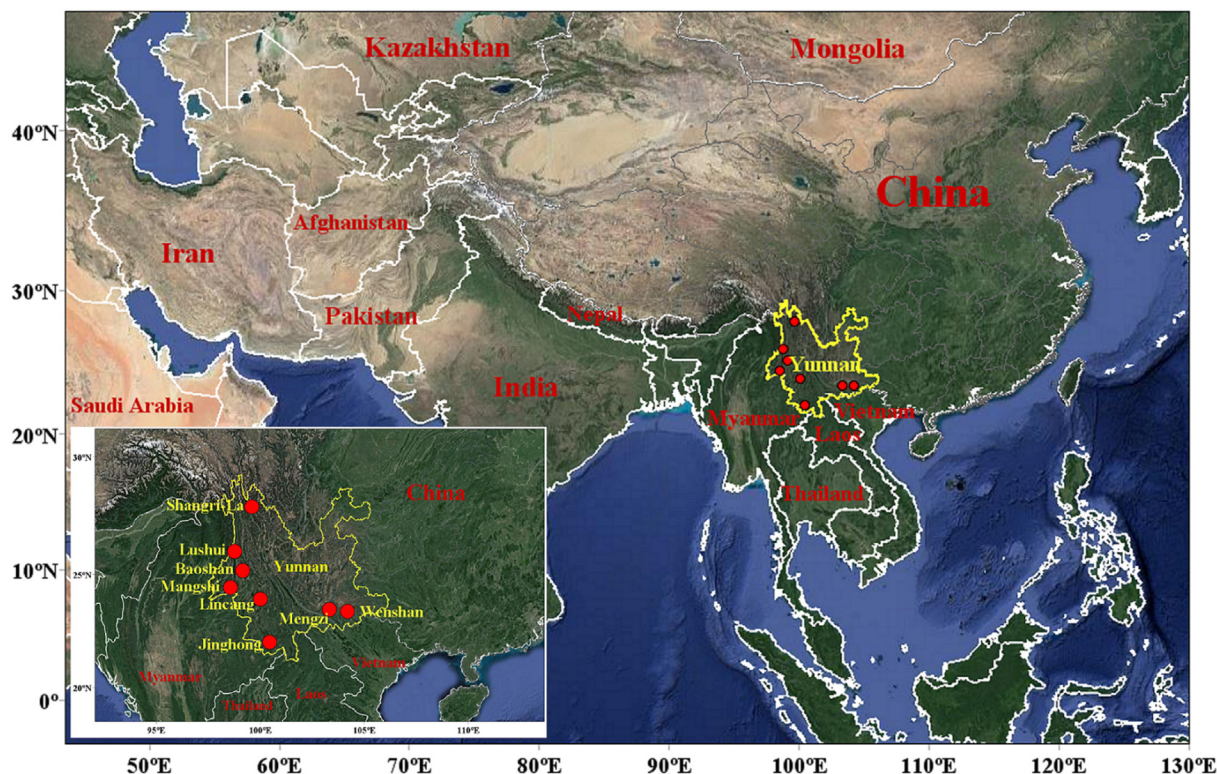


Fig. 1. Location of eight sites in Yunnan Province (Shangri-La, Lushui, Baoshan, Mangshi, Lincang, Jinghong, Mengzi, and Wenshan) in southwestern China along the border with neighboring countries Myanmar, Laos, and Vietnam.

(GDP) <30 billion RMB in 2018 (<http://stats.yn.gov.cn/>) (Table 1). These sites in Yunnan are located within 200 km from the nearest neighboring countries in Southeast Asia (Myanmar, Laos, and Vietnam) and South Asia (India).

The surface concentrations of SO₂ (sulfur dioxide), NO₂ (nitrogen dioxide), CO (carbon monoxide), O₃ (ozone), PM_{2.5} and PM₁₀ (particulate matter with an aerodynamic diameter equal to or <2.5 and 10 μm, respectively) were measured from January 2015 to December 2019 (Supplementary Data, Figs. S2–S9). Hourly mean concentrations of these six air pollutants were provided by the China National Environmental Monitoring Center (<http://106.37.208.233:20035/>).

The measurement of these six air pollutants was under the control of the state controlling air sampling sites in China. The arrangement of sites followed the technical regulation (National Environmental Protection Standards of the People's Republic of China, (HJ 664–2013). Instruments information and monitoring methods were described in Yin et al. (2019). The specifications and operation procedures of SO₂, NO₂, CO and O₃ measurements at these stations followed the national guidelines: Specifications and Test Procedures for Ambient Air Quality Continuous Auto-

ated Monitoring System prescribed in the National Environmental Protection Standards of the People's Republic of China: HJ 654–2013 for SO₂, NO₂, O₃ and CO, and HJ 653–2013 for PM₁₀ and PM_{2.5}. The inlet of the instrument was 3–20 m above the ground surface, 1 m higher than the roof of the building or the wall. The stations were located at least 50 m from any obvious stationary pollution sources. The data quality assurance and controls followed the technical guidelines on environmental monitoring quality management prescribed in the National Environmental Protection Standards of the People's Republic of China (HJ 630–2011), and the data were checked for validity based on the national ambient air quality standards of the People's Republic of China (GB 3095–2012). All data in this study are displayed in China Standard Time (CST, UTC + 8), and the local solar noon at eight sites in Yunnan is from 13:15 to 13:38 CST.

2.2. Air mass simulations and concentration weighted trajectory (CWT)

Back trajectories of air masses reaching the eight individual sites were calculated using the NOAA (U.S. National Oceanic and

Table 1
Location, population and Gross Domestic Product (GDP) of 8 cities in southwestern China in 2018.

No.	City/Province	Latitude (°N)	Longitude (°E)	Population (thousand)	Gross Domestic Product (GDP, billion RMB)
1	Shangri-La	27.82	99.71	180	13.147
2	Lushui	25.97	98.82	191	5.751
3	Baoshan	25.12	99.17	980	28.526
4	Mangshi	24.43	98.58	424	11.193
5	Lincang	23.88	100.09	340	11.544
6	Jinghong	22.01	100.48	544	21.964
7	Mengzi	23.39	103.38	458	20.825
8	Wenshan	23.37	104.24	259	24.708

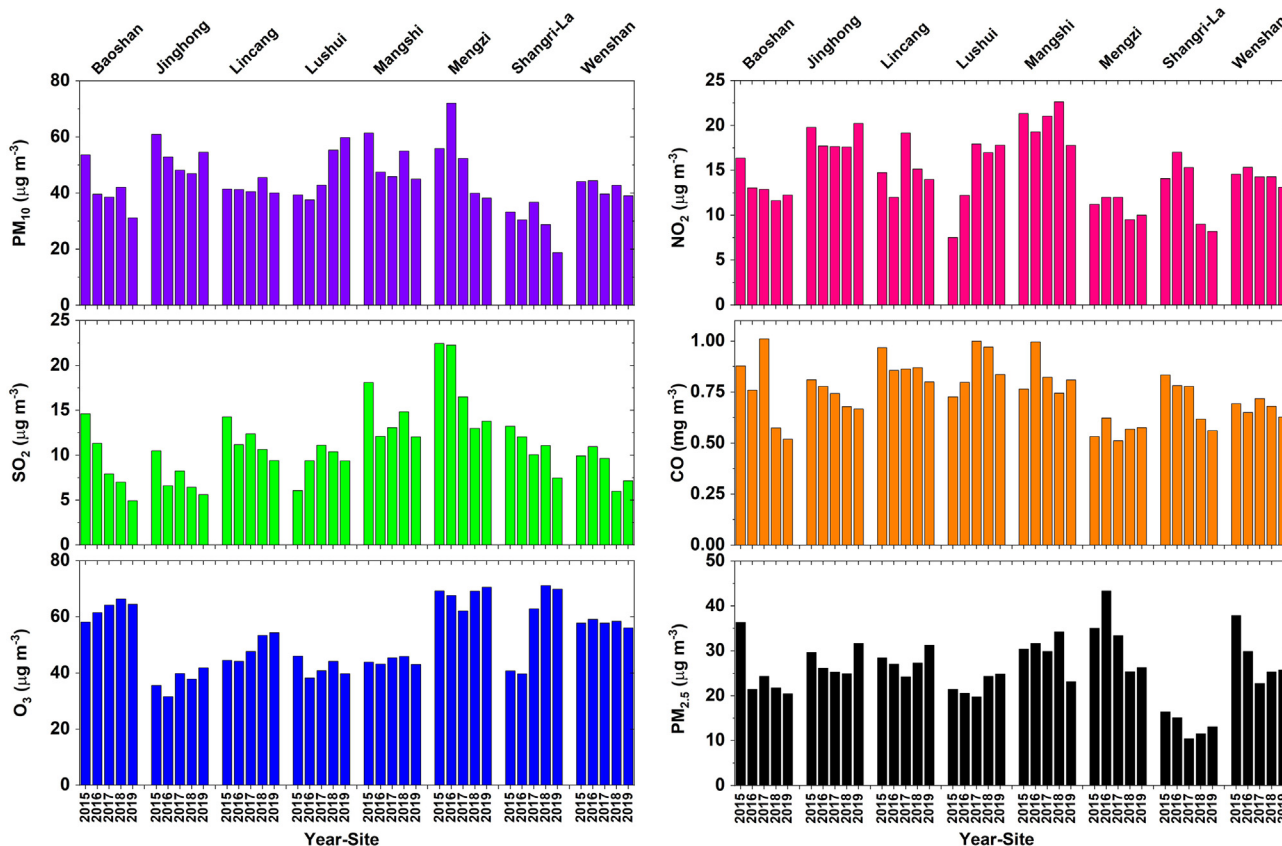


Fig. 2. Yearly mean concentrations of air pollutants observed at 8 sites in southwestern China during 2015–2019.

Atmospheric Administration) HYSPLIT (HYbrid Single-Particle Lagrangian Integrated Trajectory) model (Draxler and Rolph, 2003) by TrajStat in Meteoinfo (Wang et al., 2009; Wang, 2014). HYSPLIT is a lagrangian integrated model that can simulate air parcel trajectories to determine the transport path (how far and what direction) of air masses (Draxler and Rolph, 2003). It is widely used in studies of air mass transport. TrajStat in Meteoinfo is useful tool to simulate for HYSPLIT. The NOAA's gridded meteorological data from the Global Data Assimilation System (GDAS-1) with 23 vertical levels from 1000 hPa to 20 hPa and a horizontal resolution of 1° latitude × 1° longitude were used in HYSPLIT model in global domain. HYSPLIT model was used to simulate the air mass transport as in previous studies (Yin et al., 2018, 2020). Air masses were calculated for each year from 2015 to 2019, and similar results (e.g. air masses sources and trajectories coverage) were obtained for each year with no noticeable inter-annual changes in major directions of air masses. Therefore, air masses calculated for the full year of 2019 as representative air masses for all eight sites were used to investigate the transport of air pollutants. The total run time for each backward trajectory by the HYSPLIT was 120 h, with air mass arriving at the site at every 1 h interval, which is typically sufficient to investigate the impacts of long-range and trans-border transport of air pollutants from nearby countries. In this study, the air mass arrival height of 500 m above ground over each site was selected in the HYSPLIT calculation to represent both the long-range transport and the air mass sampled by ground-based instruments for monitoring the air pollutants in the planetary boundary layer (Yin et al., 2018).

The CWT simulation based on backward-trajectories obtained from the HYSPLIT model and in-situ measurements were used to identify the potential sources of air pollutants to the monitoring site (Seibert et al., 1994; Hsu et al., 2003). CWT simulation was carried out over eight sites for the year 2019. Here, we conducted a synthetic CWT where trajectories for all sites were used to calculate a single CWT for each air pollutant that yielded the overall potential sources of air pollutants with all sites treated as a whole. In the CWT method (Seibert et al., 1994; Hsu et al., 2003), each grid cell (a resolution of 0.5° × 0.5° in this study) is assigned a weighted

concentration by averaging the sample concentrations with associated trajectories that crossed that grid cell as follows:

$$C_{ij} = \frac{1}{\sum_{l=1}^M \tau_{ijl}} \sum_{l=1}^M C_l \tau_{ijl} \tag{1}$$

where C_{ij} is the average weighted concentration in the ij th cell, l is the index of the trajectory, M is the total number of trajectories, C_l is the concentration observed upon arrival of trajectory l , and τ_{ijl} is the time spent in the ij th cell by trajectory l . A high value of C_{ij} implies that air parcels traveling over the ij th cell were thought to be, on average, associated with high concentrations at the receptor cell. The weighting function was used in the CWT analyses to reduce the effect of small values of n_{ij} as:

$$W_{ij} \begin{cases} 1.00 & N_{ij} > 3N_{ave} \\ 0.70 & 3N_{ave} > N_{ij} > 1.5N_{ave} \\ 0.42 & 1.5N_{ave} > N_{ij} > N_{ave} \\ 0.05 & N_{ave} > N_{ij} \end{cases} \tag{2}$$

where W_{ij} represents the weight function and reflects the uncertainty of the values in each cell, N_{ij} represents the number of endpoints that fall in the ij -th cell, and N_{ave} represents the mean N_{ij} of all grid cells. The weighted CWT (WCWT) result = $W_{ij} \times$ CWT.

2.3. MODIS fire spots, CAM-chem simulations, CALIPSO, and emission inventories

The Moderate Resolution Imaging Spectroradiometer (MODIS) data provided by NASA (National Aeronautics and Space Administration) was used to understand the distribution of fire spots in the surrounding broader region. The spatial resolution of MODIS data is 1000 m × 1000 m. Daily distribution of fire spots was used in this study.

The Community Atmosphere Model with Chemistry (CAM-chem) is the atmosphere component of The Community Earth System Model with chemistry, coupled with the land model (Lamarque et al., 2012), and it was used to simulate air pollutants (Tang et al., 2019). CAM-chem uses the MOZART (Model for OZone And Related

Table 2

Five-year mean and range (min ± SD, max ± SD) of annual mean concentrations of 6 air pollutants at 8 sites in southwestern China and air quality standard for Grade I and II of each air pollutant in China.

Cities	SO ₂ (μg m ⁻³)	NO ₂ (μg m ⁻³)	CO (mg m ⁻³)	O ₃ (μg m ⁻³)	PM ₁₀ (μg m ⁻³)	PM _{2.5} (μg m ⁻³)
Baoshan (mean)	9.14 ± 10.8	13.22 ± 10.2	0.75 ± 0.46	62.99 ± 35.94	40.92 ± 28.55	24.81 ± 17.81
Baoshan (range)	4.95 ± 2.34, 14.62 ± 17.35	11.63 ± 9.11, 16.37 ± 10.93	0.52 ± 0.18, 1.01 ± 0.36	58.17 ± 36.19, 66.4 ± 35.85	31.21 ± 20.18, 53.64 ± 31.43	20.45 ± 11.51, 36.34 ± 22.46
Jinghong (mean)	7.47 ± 6.76	18.59 ± 13.28	0.74 ± 0.31	37.36 ± 36.31	52.68 ± 38.16	27.53 ± 23.25
Jinghong (range)	5.62 ± 3.15, 10.51 ± 10.04	17.6 ± 10.93, 20.24 ± 13.69	0.67 ± 0.29, 0.81 ± 0.36	31.6 ± 30.67, 41.89 ± 39.28	47.03 ± 32.14, 60.97 ± 42.19	24.93 ± 22.06, 31.64 ± 26.18
Lincang (mean)	11.57 ± 8.77	15.02 ± 9.22	0.87 ± 0.36	48.86 ± 33.95	41.77 ± 27.59	27.67 ± 17.89
Lincang (range)	9.42 ± 4.35, 14.27 ± 15.05	12 ± 9.6, 19.18 ± 11.09	0.8 ± 0.19, 0.97 ± 0.64	44.21 ± 34.48, 54.39 ± 35.7	40.06 ± 28.9, 45.6 ± 29.84	24.27 ± 17.44, 31.27 ± 17.25
Lushui (mean)	9.29 ± 5.6	14.53 ± 10.08	0.87 ± 0.39	41.82 ± 29.1	46.96 ± 28.95	22.18 ± 14.89
Lushui (range)	6.06 ± 4.52, 11.12 ± 4.1	7.53 ± 4.84, 17.94 ± 11.33	0.73 ± 0.53, 1 ± 0.27	38.31 ± 28.37, 46.07 ± 27.45	37.58 ± 24.05, 59.78 ± 33.39	19.8 ± 14.01, 24.87 ± 13.43
Mangshi (mean)	14 ± 12.62	20.4 ± 11.91	0.83 ± 0.34	44.32 ± 38.15	50.85 ± 32.92	29.87 ± 20.83
Mangshi (range)	12.05 ± 9.38, 18.12 ± 17.89	17.78 ± 10.08, 22.63 ± 13.22	0.75 ± 0.33, 1 ± 0.27	43.1 ± 35.43, 45.96 ± 37.84	44.99 ± 28.29, 61.44 ± 36.38	23.17 ± 15.63, 34.24 ± 23.77
Mengzi (mean)	17.6 ± 29.41	10.96 ± 6.49	0.56 ± 0.33	67.76 ± 32.94	51.79 ± 33.02	32.74 ± 22.56
Mengzi (range)	12.99 ± 13.04, 22.45 ± 41.31	9.51 ± 5.18, 12 ± 9.6	0.51 ± 0.28, 0.62 ± 0.49	62.15 ± 32.2, 70.65 ± 31.74	38.22 ± 24.07, 72.09 ± 37.14	25.37 ± 17.58, 43.37 ± 24.1
Shangri-La (mean)	10.77 ± 8.02	12.76 ± 8.04	0.71 ± 0.41	56.91 ± 27.49	29.62 ± 18.86	13.32 ± 8.23
Shangri-La (range)	7.46 ± 4.42, 13.23 ± 8.63	8.22 ± 5.2, 17.03 ± 7.75	0.56 ± 0.23, 0.83 ± 0.5	39.69 ± 19.89, 71.2 ± 27.54	18.83 ± 12.42, 36.77 ± 21.31	10.43 ± 7.9, 16.46 ± 7.78
Wenshan (mean)	8.76 ± 10.49	14.32 ± 7.29	0.67 ± 0.25	57.84 ± 30.11	42.01 ± 27.24	28.26 ± 18.57
Wenshan (range)	5.99 ± 6.38, 10.97 ± 14.03	13.12 ± 5.9, 15.33 ± 8.91	0.63 ± 0.2, 0.72 ± 0.23	56.08 ± 28.87, 59.12 ± 32.07	39.07 ± 25.14, 44.48 ± 27.41	22.73 ± 16.47, 37.86 ± 18.49
China Grade-I	20 ^a	40 ^a	4 ^b	160 ^c	40 ^a	15 ^a
China Grade- II	60 ^a	40 ^a	4 ^b	200 ^c	70 ^a	35 ^a

^a: annual mean, ^b: daily mean, and ^c: hourly mean.

chemical Tracers) chemical mechanism, with various choices of complexity for tropospheric and stratospheric chemistry. The horizontal resolution for CAM-chem is $0.5^\circ \times 0.5^\circ$, and the CAM-chem simulation results used in this study is in global domain.

The Cloud-Aerosol Lidar and Infrared Pathfinder Satellite Observation (CALIPSO) (<https://www-calipso.larc.nasa.gov>) data provided by the NASA and CNES (Centre National d'Etudes Spatiales) were used to investigate the distribution of atmospheric aerosols. The Cloud-Aerosol Lidar with Orthogonal Polarization (CALIOP) is a space-borne Lidar instrument on board the CALIPSO satellite that provides high-resolution vertical profiles of aerosols and clouds. The horizontal resolution of CALIOP is 333 m and the vertical resolution is 30 m. CALIPSO retrieved backscatter signal on March 31st 2019 was used in this study.

In order to explore the emission distributions in the region and help with the interpretation of the observations, the monthly total

emission inventories with $0.1^\circ \times 0.1^\circ$ spatial resolution for SO_2 , NO_2 , CO, PM_{10} , and $\text{PM}_{2.5}$ were obtained from the Peking University Emission Inventory (2014, which is the most updated inventory provided by Peking University Emission Inventory) (<http://inventory.pku.edu.cn/download/download.html>) (Huang et al., 2014, 2017; Zhong et al., 2017), and later used as annual total emission (Supplementary Data, Fig. S10).

3. Results and discussion

3.1. Overview of gaseous and particulate pollutants in southwestern China

The annual mean concentrations of six pollutants during 2015–2019 are shown in Fig. 2. Mean SO_2 concentrations (of all eight sites, unless otherwise stated in this section) over the obser-

Table 3
Inter-annual trends of air pollutants at 8 sites in southwestern China during a 5-year period 2015–2019.

City	SO_2 ($\mu\text{g m}^{-3} \text{ year}^{-1}$)	NO_2 ($\mu\text{g m}^{-3} \text{ year}^{-1}$)	CO ($\text{mg m}^{-3} \text{ year}^{-1}$)	O_3 ($\mu\text{g m}^{-3} \text{ year}^{-1}$)	PM_{10} ($\mu\text{g m}^{-3} \text{ year}^{-1}$)	$\text{PM}_{2.5}$ ($\mu\text{g m}^{-3} \text{ year}^{-1}$)
1 Shangri-La	-1.07***	-1.74***	-0.06***	8.30***	-3.19***	-1.13***
2 Lushui	0.68*	2.70***	0.03+	-0.66	5.99***	1.14***
3 Baoshan	-2.13***	-0.76*	-0.07***	1.88*	-4.97***	-2.22*
4 Mangshi	-0.34	-0.64**	-0.01	0.29	-3.41***	-1.55*
5 Lincang	-0.96***	0.07	-0.02	2.74***	-0.71	0.41
6 Jinghong	-0.90***	0.16	-0.03***	2.03**	-2.18**	-0.06
7 Mengzi	-2.18***	-0.42**	0.01	0.78	-7.33***	-3.50***
8 Wenshan	-0.81***	-0.32*	0	0.31	-0.99	-2.47***

($p < 0.001 = \text{***}$, $p < 0.01 = \text{**}$, $p < 0.05 = \text{*}$ and $p < 0.1 = \text{+}$).

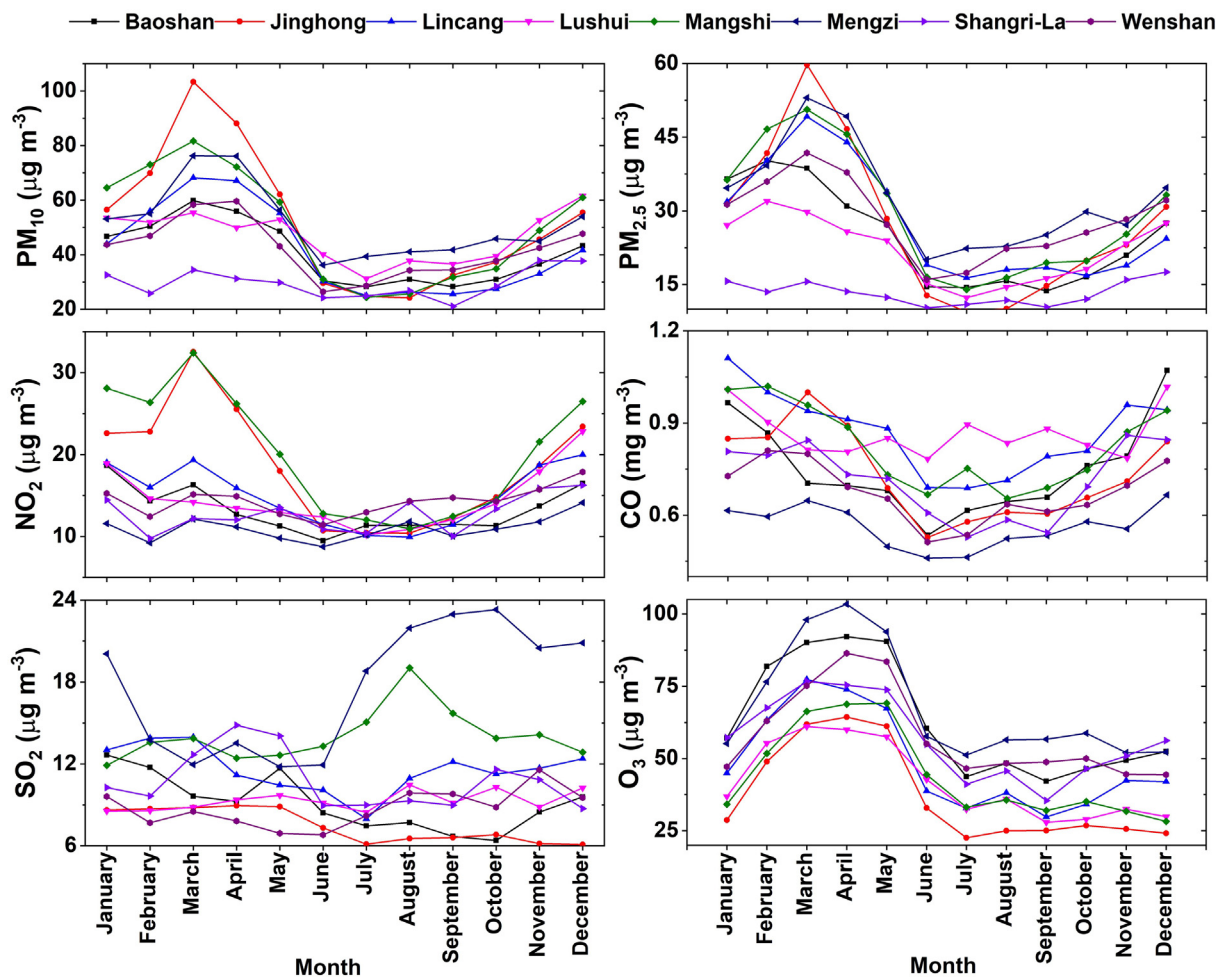


Fig. 3. Monthly mean concentrations of air pollutants observed at 8 sites in southwestern China during 2015–2019.

vation period of 5 years ranged from $7.47 \pm 6.76 \mu\text{g m}^{-3}$ (Jinghong) to $17.6 \pm 29.41 \mu\text{g m}^{-3}$ (Mengzi) (Table 2), and annual concentrations at all sites met the China Grade-I standard for the annual mean SO_2 concentration ($20 \mu\text{g m}^{-3}$). For NO_2 , the mean concentrations ranged from $10.96 \pm 6.49 \mu\text{g m}^{-3}$ (Mengzi) to $20.4 \pm 11.91 \mu\text{g m}^{-3}$ (Mangshi), with annual mean concentrations over eight sites were within the China Grade-I standard for the annual mean NO_2 concentration ($40 \mu\text{g m}^{-3}$). In case of CO, the mean concentrations ranged from $0.56 \pm 0.33 \text{mg m}^{-3}$ (Mengzi) to 0.87mg m^{-3} (Lincang and Lushui). Likewise for O_3 , the mean concentrations were from $37.36 \pm 36.31 \mu\text{g m}^{-3}$ (Jinghong) to $67.76 \pm 32.94 \mu\text{g m}^{-3}$ (Mengzi). The PM_{10} mean concentrations were in the range from $29.62 \pm 18.86 \mu\text{g m}^{-3}$ (Shangri-La) to $52.68 \pm 38.16 \mu\text{g m}^{-3}$ (Jinghong) whereas the $\text{PM}_{2.5}$ mean concentrations were in the range from $13.32 \pm 8.23 \mu\text{g m}^{-3}$ (Shangri-La) to $32.74 \pm 22.56 \mu\text{g m}^{-3}$ (Mengzi). Interestingly, among eight sites, Shangri-La was the only site where the China Grade-I standards for the annual mean PM_{10} concentration ($40 \mu\text{g m}^{-3}$) and the annual mean $\text{PM}_{2.5}$ concentration ($15 \mu\text{g m}^{-3}$) were met while the other sites met the China Grade-II standards for PM_{10} ($70 \mu\text{g m}^{-3}$) and $\text{PM}_{2.5}$ ($35 \mu\text{g m}^{-3}$). Among all sites, concentrations of all individual six air pollutants were almost comparable, which may be due to the influence of same/similar emissions (e.g., pollution of regional scale) and similar atmospheric conditions across the cities. This is an indication of regio-

nal scale pollution covering a large area under the same regional meteorological and emission regimes. The relatively low concentrations of particulate pollutants at Shangri-La may be due to its remote location on the edge of the Tibetan Plateau. Compared with previous studies at sites in China (Wang et al., 2014; Zhao et al., 2016; Yin et al., 2017; Rupakheti et al., 2021), concentrations of both gaseous (except O_3) and particulate pollutants at eight sites in this study were at a low concentrations, while concentrations of O_3 were comparable.

Table 3 summarizes the inter-annual trends in ambient concentrations of air pollutants during a 5-year observation period from 2015 to 2019. At Shangri-La, Baoshan, and Mangshi, concentrations of all pollutants except O_3 decreased. However, Lushui showed opposite trends that all pollutants except O_3 increased. The SO_2 , NO_2 , PM_{10} , and $\text{PM}_{2.5}$ concentrations at both Mengzi and Wenshan showed decreasing trends while O_3 had an increasing trend and CO had no trend. In Lincang, three pollutants viz. SO_2 , CO, and PM_{10} exhibited decreasing trends, and other three pollutants exhibited increasing trends. Jinghong had similar trends as in Lincang except for $\text{PM}_{2.5}$ which showed decreasing trend. The trends at these sites indicated that the concentrations of air pollutants over this part of China have in general reduced. However, O_3 concentrations increased at seven sites, with Shangri-La having an exceptionally high increasing rate of $8.30 \mu\text{g m}^{-3} \text{year}^{-1}$ over a five year period. A similar trend in O_3 concentration has also been reported at many

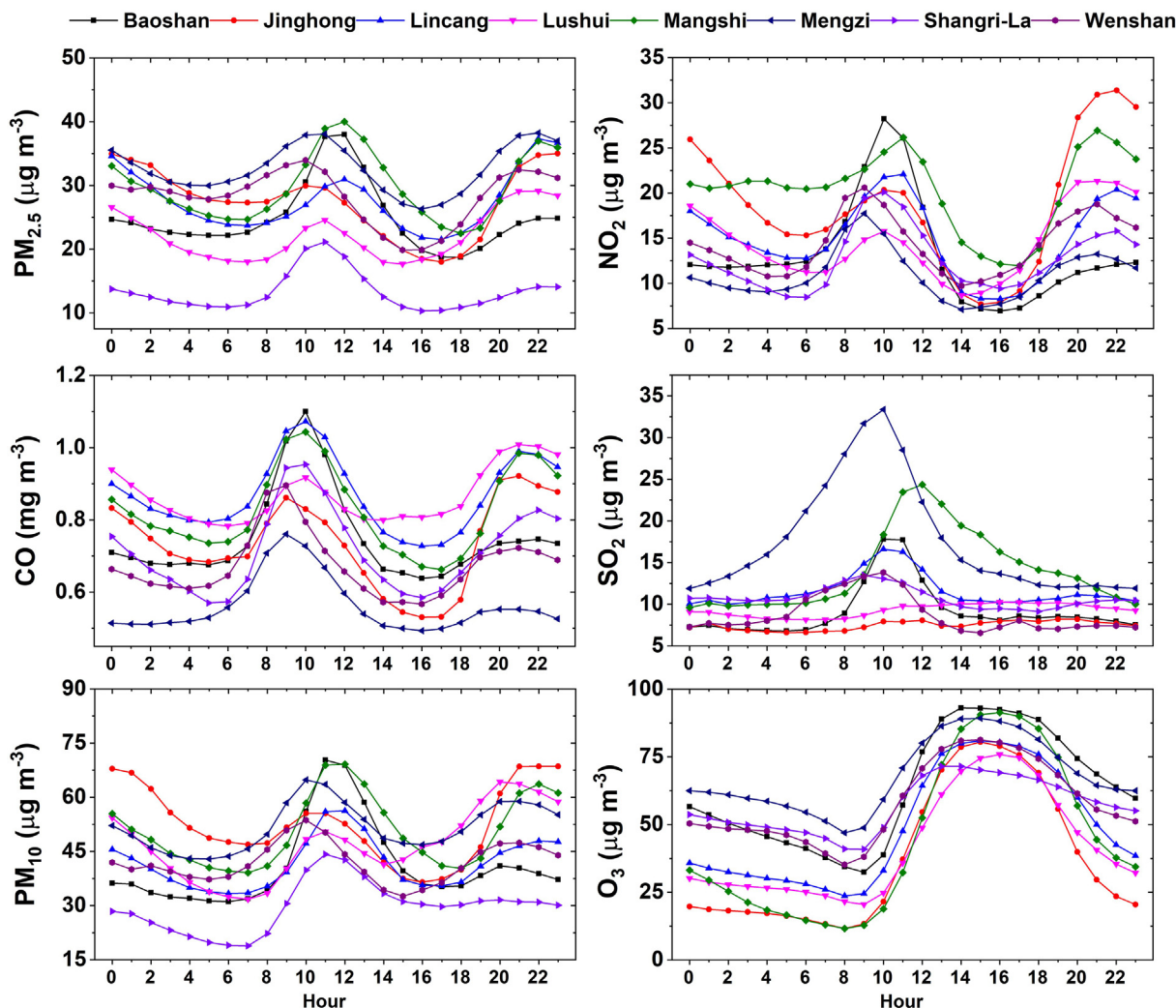


Fig. 4. Diurnal variations of air pollutants observed at 8 sites in southwestern China during 2015–2019.

other locations in China, which is mostly attributed to the changes in emissions of VOCs (volatile organic compounds) and NO_x (Ma et al., 2016; Lu et al., 2020).

3.2. Monthly variations of air pollutants

Fig. 3 shows the monthly mean concentrations of air pollutants during 2015–2019. For SO₂, there was no uniform monthly variation across eight sites. The monthly mean SO₂ concentrations at Shangri-La peaked in April and reached its second peak in October. At Baoshan, the monthly mean SO₂ concentrations peaked first in January and later in May. At Lushui, no pronounced peak of SO₂ was found. For other sites, the monthly mean concentrations of SO₂ peaked in different months (Wenshan: in November; Mengzi: in October; Mangshi: in August; Lincang: in March; Jinghong: in May). Different from this study, Zhao et al. (2016) found the monthly mean concentrations of SO₂ at provincial capital cities in China generally peaked in the winter in northern China, due to more coal combustion for domestic heating and poor meteorological conditions such as low boundary layer height, weak wind, and less precipitation. Whereas in southern cities without winter heating, the seasonal variations of SO₂ concentration were weak (Yin et al., 2017). For NO₂, monthly mean concentrations at five sites (Shangri-La, Wenshan, Lushui, Mengzi, and Lincang) reached their peaks in December. The monthly mean concentration of NO₂ at Baoshan peaked in January. At Mangshi and Jinghong, the monthly mean concentrations of NO₂ peaked in March. Most of the sites observed NO₂ peaks during winter. In most provincial capital cities in China, monthly mean NO₂ concentrations peaked in winter, similar to six sites in this study, which was caused by combined effects of weather conditions (e.g. weak winds and shallow mixing layers) and primary emissions (Zhao et al., 2016; Yin et al., 2017). The CO peaks were observed during December at Lushui, Baoshan, and Mengzi, during November at Shangri-La, and during February at

Wenshan and Mangshi. At Lincang, the monthly mean CO peaked in January. The monthly mean CO at Jinghong peaked in March. In this study, monthly mean CO concentration at different sites peaked in the winter, early spring, or late autumn (in January at Lincang), which was different from the results at provincial capital cities in China where CO concentrations peaked in January (Yin et al., 2017), and it may due to the long-range transport of CO from South Asia (see section 3.5).

For O₃, all sites showed uniform intra-annual variation across sites with their monthly mean concentrations of O₃ peaked in the spring months. O₃ at the surface is generally formed through photochemical reactions between NO_x and VOCs (Atkinson, 2000). Zhao et al. (2016) found that O₃ concentrations were high in the summer and negatively correlated with concentrations of pollutants (CO and NO_x) emitted from combustion activities. O₃ is a secondary pollutants and its formation rate depends strong on intensity of solar radiation. Unlike previous studies at most urban sites in China, spring peaks in O₃ concentrations in this study were similar to the high O₃ concentration in the spring in the southern Tibetan Plateau (Yin et al., 2017, 2019; Duo et al., 2018), where the monthly O₃ concentration variation was largely controlled by the intrusion of ozone from stratosphere.

For maximum PM₁₀, monthly mean concentrations of PM₁₀ at Shangri-La and Lushui were observed in December, whereas during March at Baoshan, Mengzi, Mangshi, Lincang, and Jinghong and during April in Wenshan. Most sites reached their PM₁₀ peaks in the spring. The monthly mean concentration of PM_{2.5} peaked in December (Shangri-La), in March (Wenshan, Mengzi, Mangshi, Lincang, and Jinghong), and in February (Lushui and Baoshan). Monthly mean concentrations of PM_{2.5} at sites in this study peaked either in winter or in spring. Peaks of particulate pollutants at urban sites mostly occurred in the winter owing to the impacts of enhanced local emissions (e.g., home heating) under the calm atmospheric conditions that are not conducive to diffusion and

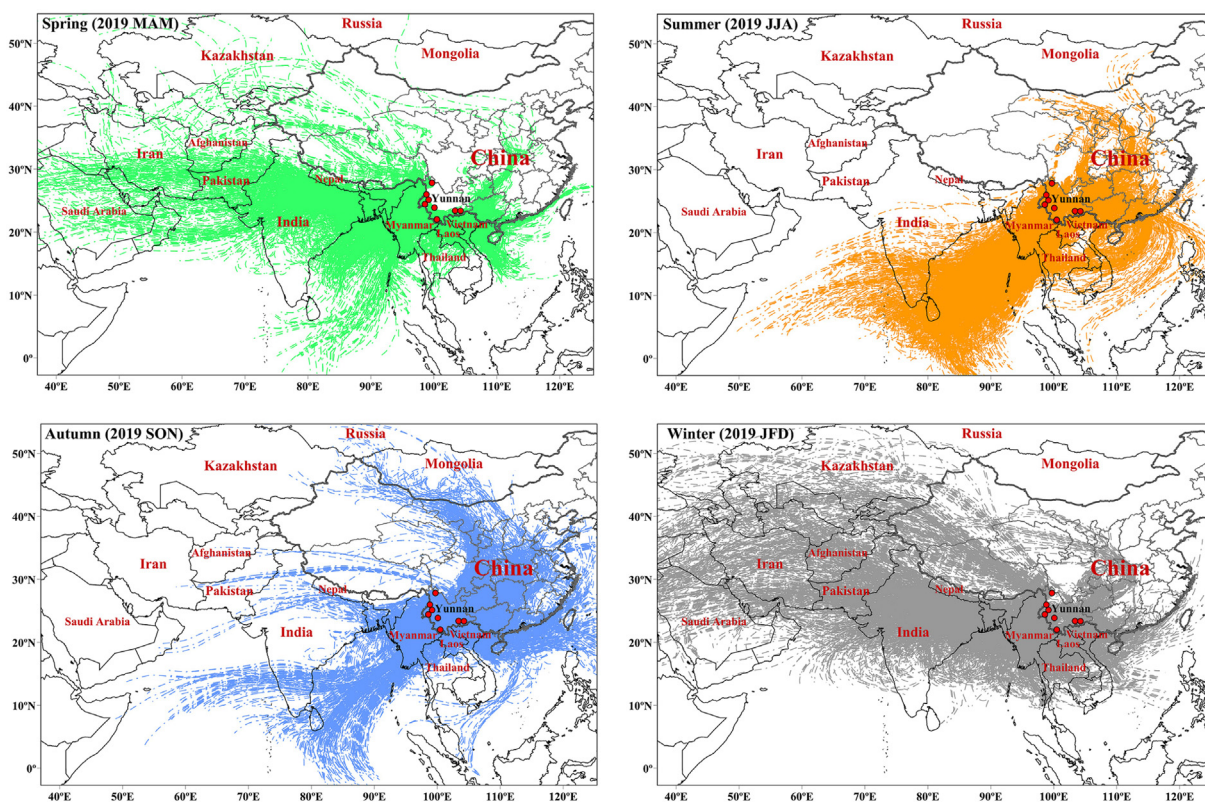


Fig. 5. Backward trajectories showing the air masses arriving at the 8 sites in southwestern China by season for 2019.

dilution of pollutants. Some cities in northern and northwestern China showed their PM_{2.5} maximum in the spring due to the impact of dust plumes from Asian deserts (Yin et al., 2017; Rupakheti et al., 2021). In this study, six (five) sites reached their PM₁₀ (PM_{2.5}) peaks in the spring, which is different from those at most provincial capital cities in China probably caused by transported pollution plumes (which is explored in the following section) in addition to local sources.

3.3. Diurnal variations of air pollutants

Diurnal variations of air pollutants at eight sites in southwestern China during 2015–2019 are shown in Fig. 4. The diurnal variations of air pollutants in this study were similar to those in provincial cities (Zhao et al., 2016; Yin et al., 2017). The O₃ concentrations at all eight sites showed a single peak with maximum in the afternoon

and minimum in the morning (Fig. 4). Enhanced photochemical production and potential intrusion the air mass with higher O₃ in free troposphere to surface probably contributed to the high O₃ concentration in the afternoon. For other pollutants, the diurnal variations are characterized by bimodal peaks occurred in the morning and late afternoon that coincided with the traffic rush hours under meteorological conditions conducive of accumulation of pollution (e.g. low boundary layer height and low wind speed) and enhanced anthropogenic activities; low concentrations in the afternoon owing to good dispersion and dilution conditions due to high wind speed and high boundary layer height (Zhao et al., 2016).

3.4. Air mass transport to the sites

During 2019, the study area was generally under the influence of westerly or southwesterly winds and partly under the easterly

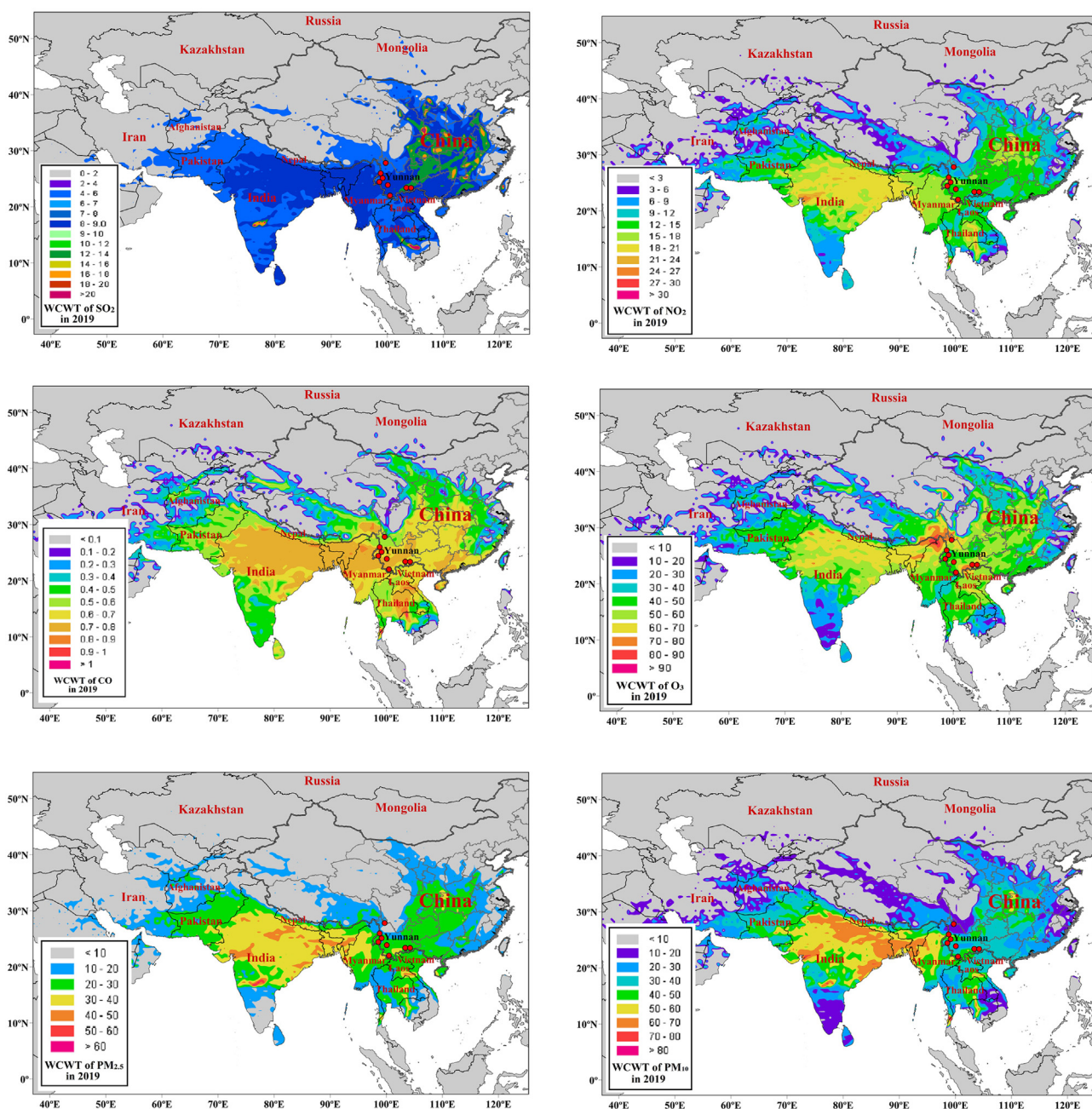


Fig. 6. Concentration weighted trajectory (CWT) of 6 air pollutants (SO₂, NO₂, CO, O₃, PM₁₀ and PM_{2.5}) at 8 sites in southwestern China in 2019.

or northeasterly winds (in August and September) at 500 hPa. The backward trajectories of air masses (with their history over 5 days tracked) arriving at the eight sites in 2019 are shown in Fig. 5. In spring, most air masses originated in or passed over South Asia (e.g., India, Nepal, and Pakistan) and Southeast Asia (e.g., Myanmar, Laos, Thailand, and Vietnam). Only a few trajectories were originated in China (e.g., Guangxi Province, Guizhou Province, and Hunan Province) in this season. During summer, the contribution of air mass from continental South Asia reduced, and most trajectories were originated over the Bay of Bengal and Southeast Asia. In autumn, trajectories from the Bay of Bengal were less than those in summer, and most trajectories originated or through the southwestern and southern China. Furthermore, there were still a lot of air masses from Southeast Asia in autumn. Interestingly, winter trajectories were similar to those in the spring, such that most trajectories originated from South Asia and Southeast Asia. In all, air

masses arriving at the sites in this study mostly originated from South Asia and Southeast Asia in spring and winter, and Southeast Asia and China in the summer and autumn.

3.5. Potential sources of air pollutants

Potential sources were calculated only for one full year (2019) to avoid double-counting of contribution from the same source in different years. Fig. 6 shows the CWT calculation results of six air pollutants at eight sites in 2019. For SO₂, the high potential sources (in high WCWT) regions were focused on central China (Fig. 6), which is in accord with the emission inventory of SO₂ (Supplementary Data, Fig. S10), indicating significant emission of SO₂ in China. The locations of eight sites were not identified as high potential sources due to the low emission of SO₂ in this region because of the low industrial activities in southwestern China

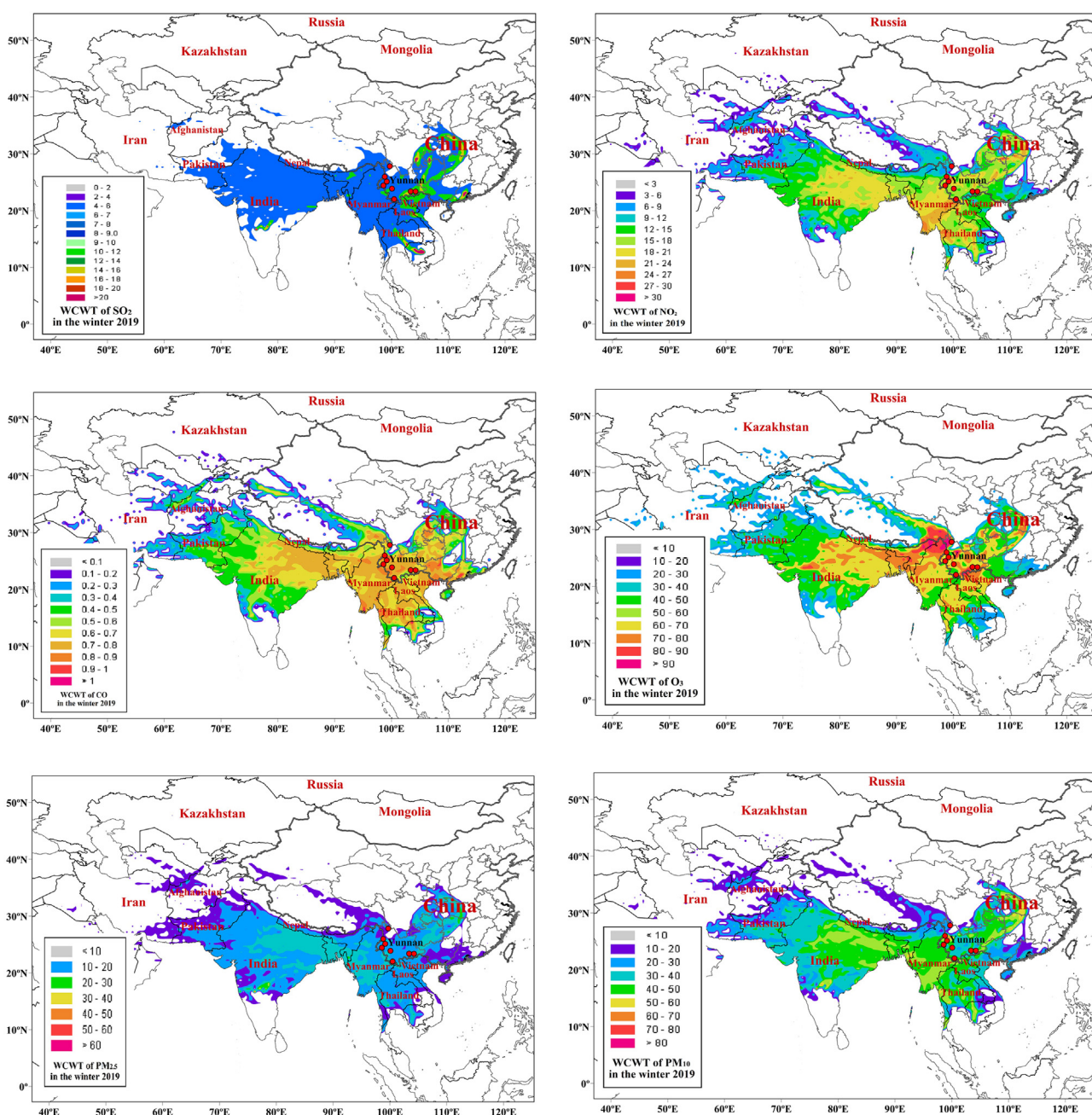


Fig. 7. Concentration weighted trajectory (CWT) of 6 air pollutants (SO₂, NO₂, CO, O₃, PM₁₀ and PM_{2.5}) at 8 sites in southwestern China in the winter 2019.

(Supplementary Data, Fig. S10). As 80% of NO_x was generally in NO_2 form, the emission inventory of NO_x was investigated in this study. India (mostly northern central India), Myanmar, Thailand, and central China were identified as high potential sources of NO_2 (Fig. 6). Almost all these high potential source areas of NO_2 were in the high NO_x emission region (Supplementary Data, Fig. S10). For CO, India, Myanmar, Bangladesh, Thailand, Laos, Vietnam, and the local areas in southwestern China and central China were identified as high potential sources (Fig. 6). The emission of CO in the study region was relatively high compared with the emission of NO_2 and SO_2 (Supplementary Data, Fig. S10), probably due to the biomass burning in this area (Qin and Xie, 2011; Qin et al., 2014). Potential source regions were similar for both fractions of particulate pollutants (Fig. 6), mostly from South Asian countries (such as India and Bangladesh) and central China. However, for O_3 , the southwestern Tibetan Plateau was identified as the most signifi-

cant potential source (Fig. 6). O_3 is a secondary pollutant formed by photochemical reactions between NO_x and VOCs in presence of sunlight. Besides photochemical reaction, the input of O_3 from the stratosphere and free troposphere is another crucial source of surface ozone, more so in the high altitude regions (e.g., Luo et al., 2019), which lead to the high O_3 concentrations at sites in the Tibetan Plateau where the stratospheric intrusion frequently happens (Chen et al., 2011; Yin et al., 2017; Luo et al., 2019). The calculation of potential sources of O_3 indicated that the high O_3 concentrations in the Tibetan Plateau might affect the O_3 concentration in southwestern China (largely influenced by the stratospheric intrusion over large region).

For NO_2 and CO, peaks of these two air pollutants' monthly mean concentrations were mostly in the winter. CWT of air pollutants in the winter of 2019 is presented as Fig. 7. In winter, regions including India, Myanmar, Thailand, southwestern and central

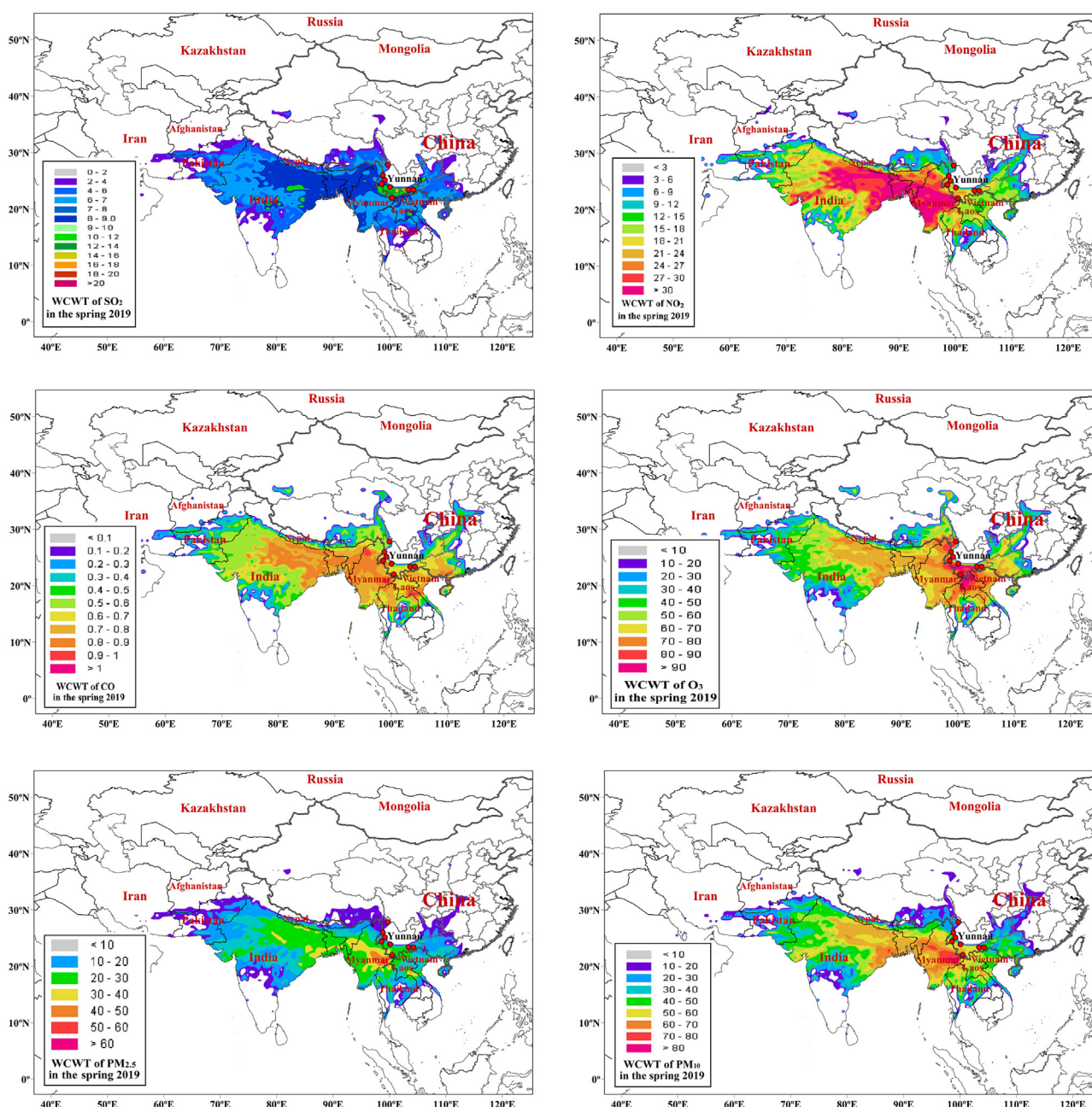


Fig. 8. Concentration weighted trajectory (CWT) of 6 air pollutants (SO_2 , NO_2 , CO, O_3 , PM_{10} and $\text{PM}_{2.5}$) at 8 sites in southwest China in the spring 2019.

China were associated with high concentrations of NO₂. For CO, India, Myanmar, Laos, Thailand, Vietnam, southwestern and southern China were associated with high concentrations of CO. For PM₁₀ and PM_{2.5}, peaks of monthly mean concentrations of these three air pollutants were mostly in the spring (Fig. 8) associated with air masses from India and Myanmar, whereas the influence of PM₁₀ and PM_{2.5} from inland China is limited. For O₃, besides the impact from the Tibetan Plateau, the effects from the local area and adjacent areas were evident in the spring (Figs. 7 and 8).

In summary, air pollutants, including NO₂, CO, PM₁₀, and PM_{2.5}, at eight sites in southwestern China were mainly affected by South Asia, Southeast Asia, and slightly from China. The concentrations of SO₂ at eight sites in southwestern China were primarily influenced by the air masses from central China. O₃ concentrations were associated mainly with the air masses coming from the Tibetan Plateau. Local emissions of air pollutants in the area where eight sites are located had a limited contribution to the high concentrations of air pollutants in this study. The transboundary transport of air pollutants from South Asia and Southeast Asia significantly influenced the concentrations of air pollutants on the southwestern border of China.

3.6. Two air pollution episodes

In this study, we analyzed two types of episodes governed by two different processes: local emissions and long-range transport. Episode 1 happened right after midnight in the night of February 4th, 2019, which was the Chinese Lunar New Year's Eve (Fig. 9). High concentrations of PM₁₀, PM_{2.5}, and SO₂ were recorded by the ground measurements, with the highest hourly concentrations recorded at 01:00 on February 5th, 2019. At Jinghong, the hourly concentration of SO₂ at 1:00 on February 5th, 2019, was 140 μg m⁻³, which was more than 20 times the monthly mean concentration in February 2019 (5.94 μg m⁻³). The mean concentration of SO₂ at eight sites at 1:00 on February 5th, 2019 was 15 times higher than the average of those in February 2019, indicating a significant episode of SO₂ occurred in this region in the eve of the Chinese New Year, clearly indicating massive local emissions. Besides SO₂, PM₁₀ and PM_{2.5} were also increased during this episode. The fireworks on New Year's Eve were the most critical contributor to these air pollutants' elevated concentrations. Even though many big cities in China have banned fireworks in urban areas, the small cities, as in this study, still maintain the custom of setting off a

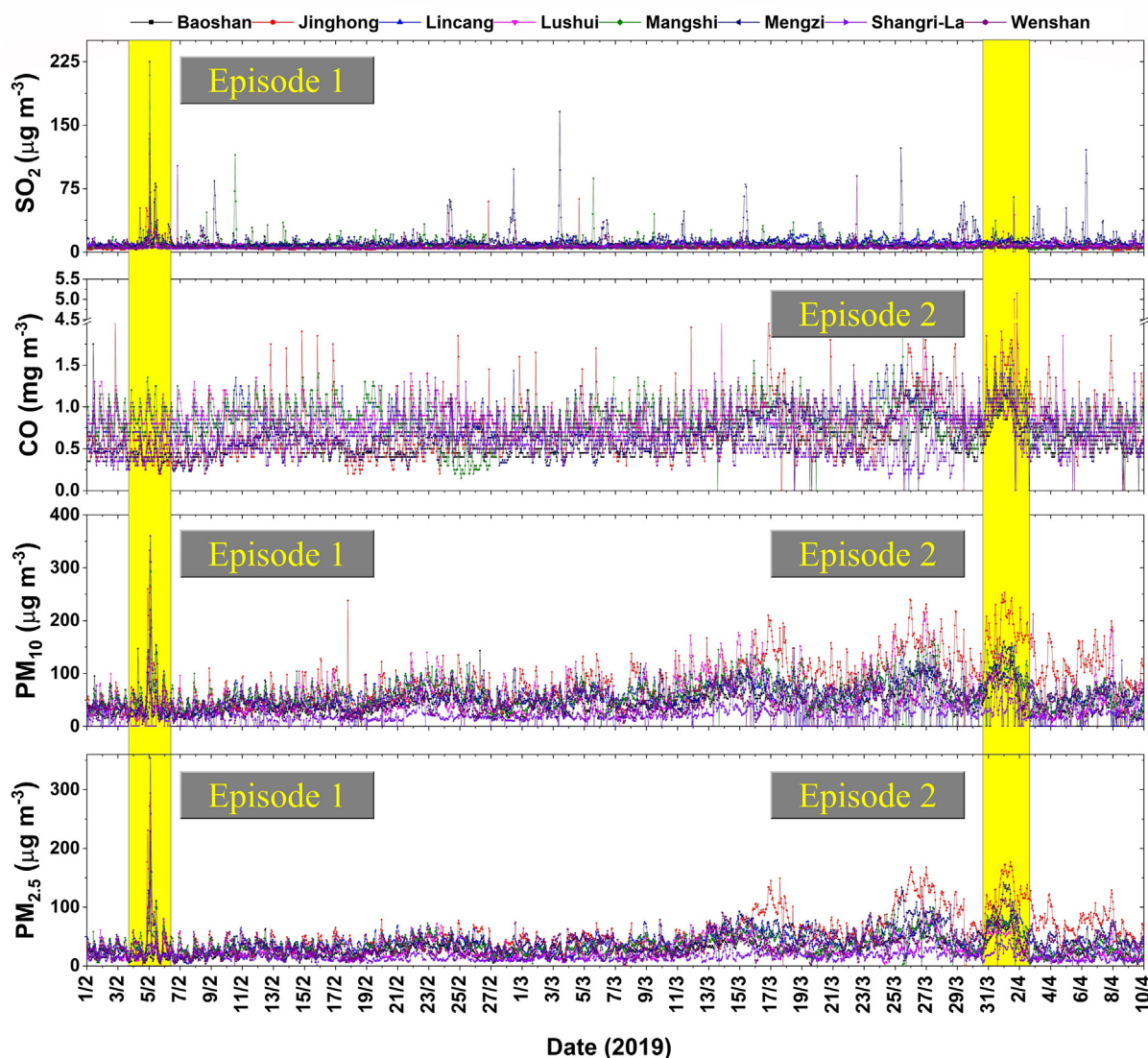


Fig. 9. Episodes of air pollutants observed across 8 sites in southwestern China.

large number of fireworks on New Year's Eve to celebrate the New Year. It's worth noting that the concentrations of PM₁₀, PM_{2.5}, and SO₂ decreased back to typically normal concentrations in a few hours (4–8 hrs), as local emissions from fireworks are short-term and high-concentrated.

Episode 2 occurred during March 31st - April 1st, 2019, with high concentrations of PM₁₀, PM_{2.5}, and CO. Compared with the Episode 1, the Episode 2 showed a relatively smaller increase (about 1.5–2 times the monthly average) in concentration of air pollutants (PM₁₀, PM_{2.5}, and CO) at all sites, while the later episode lasted longer than the former one. Almost all pollutants had clearly

higher baseline (background) concentrations at all sites, indicating a regional scale pollution episode. Hourly backward trajectories during Episode 2 are shown in Fig. 10 during which, air masses transported the emissions from South Asia via transboundary transport. The aerosol vertical distribution achieved by Cloud-Aerosol Lidar with Orthogonal Polarization (CALIOP) is shown in Fig. 11. It is demonstrated that Southeast Asia countries (e.g., Myanmar) are covered by thick smoke and polluted dust layer during Episode 2. It can be concluded that before reaching southwestern China, the air masses passed through the regions with high concentrations of air pollutants (PM_{2.5} and CO) in South Asia

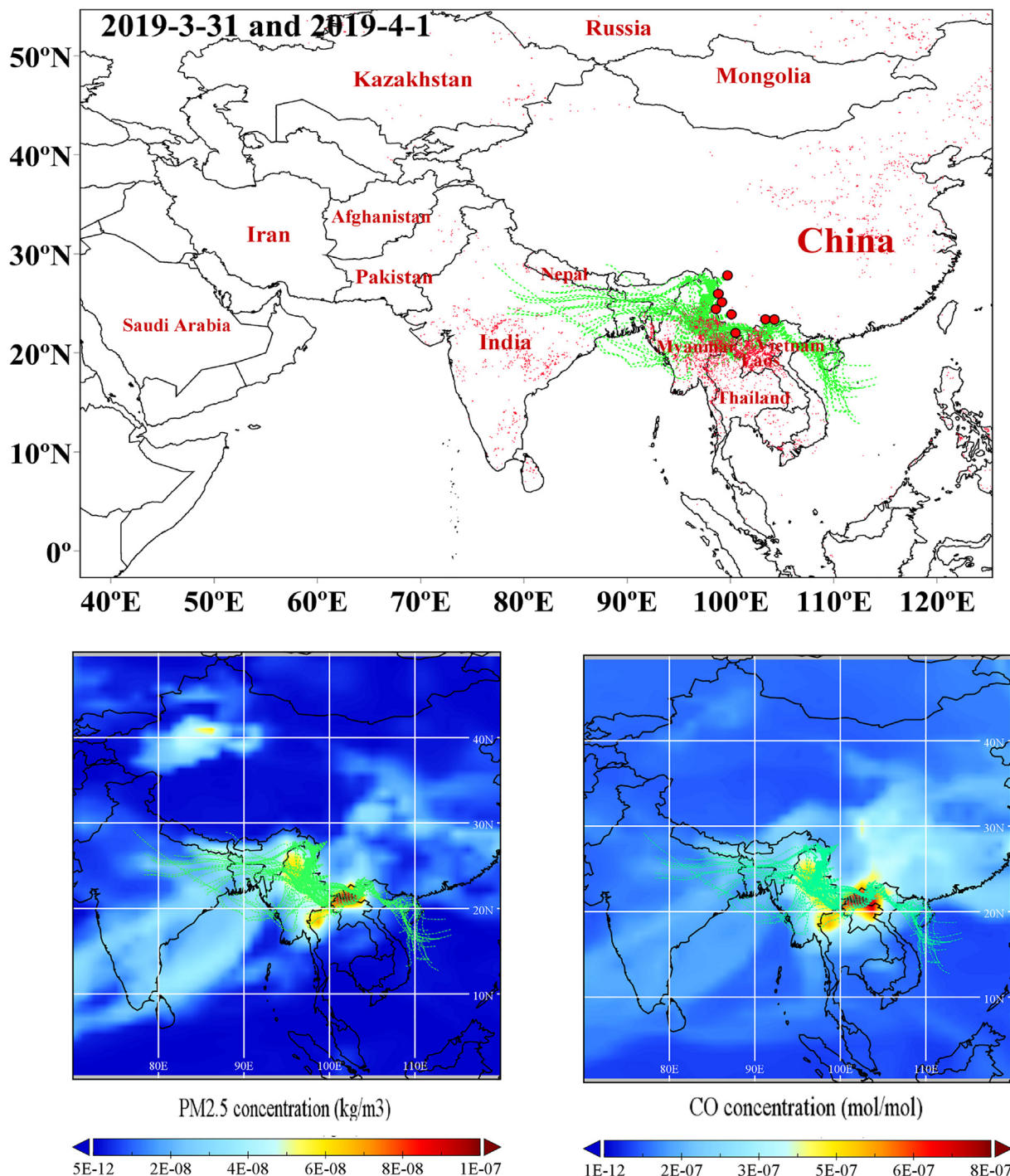


Fig. 10. Hourly back trajectories (120 h) of air masses arriving at eight sites and fire spots from MODIS C6 (top panel), the surface level (810 hPa) PM_{2.5} concentration (bottom left panel) and CO concentration (bottom right panel) from CAM-chem (bottom) simulations during the air pollution episode 2 (March 31st to April 1st, 2019) in the region.

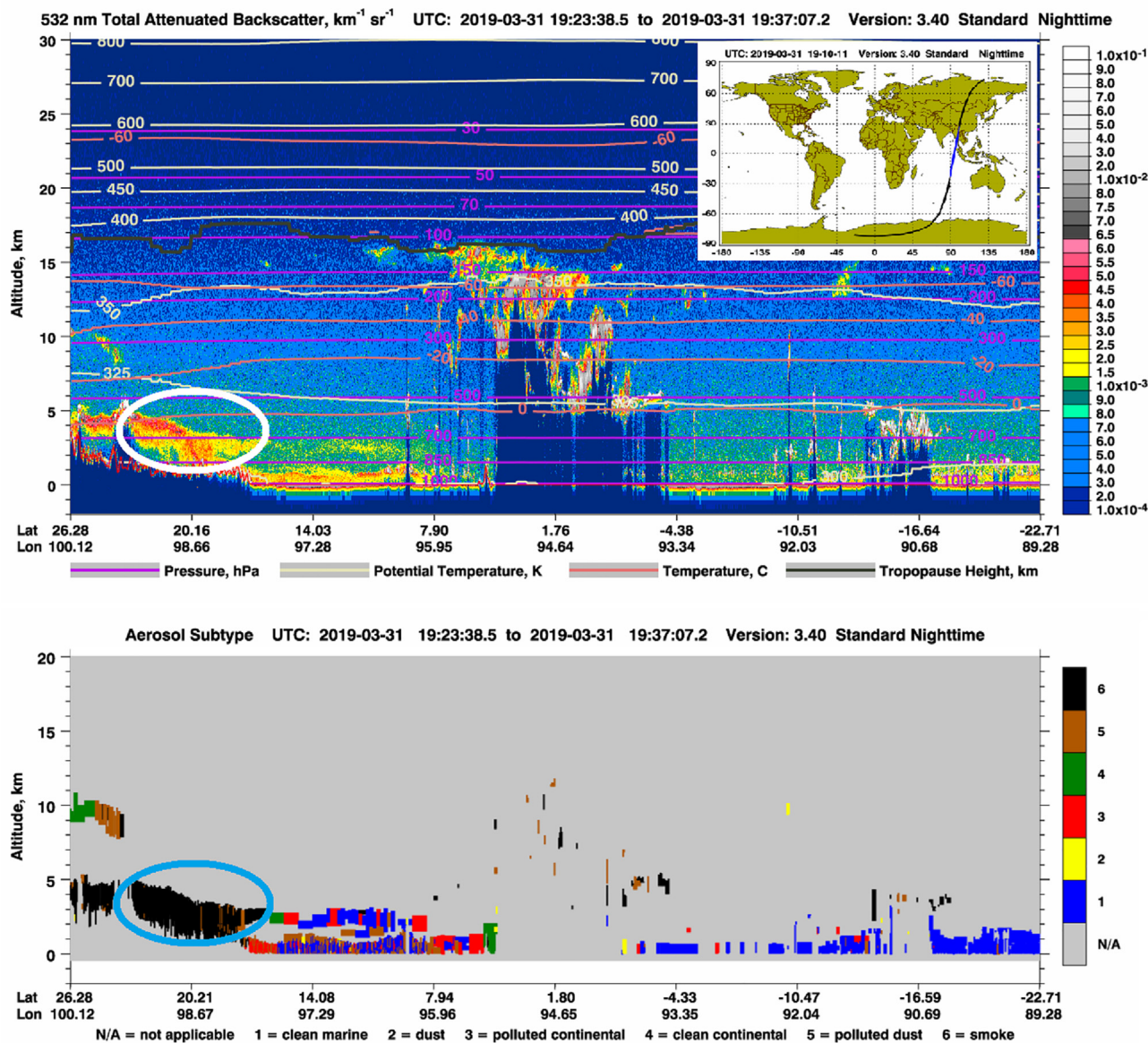


Fig. 11. CALIPSO retrieved backscatter signal at 532 nm (top) and aerosol sub-type information (bottom) on March 31st 2019. The countries in South Asia (e.g. Myanmar) are covered by a thick smoke layer (marked with circles).

(Fig. 10), ultimately bringing in transboundary emissions to Yunnan and impacting the air quality at eight sites.

4. Conclusions

The characteristics of several gaseous and particulate pollutants were investigated at eight sites from January 2015 to December 2019 in previously unreported region of southwestern China. Levels of pollutants, their temporal variations, and potential sources/source regions were analyzed. Most sites considered in this study met the China Grade-I standard of SO₂, NO₂, and the China Grade-II standard of PM₁₀ and PM_{2.5}. Concentrations of CO and O₃ at observed eight sites in this study were comparable with those in cities in China. For most sites, concentrations of air pollutants (SO₂, NO₂, CO, PM₁₀, and PM_{2.5}) experienced decreasing trends, while O₃ concentrations increased (7 of 8 sites) over the period of five years.

Monthly mean concentrations of most air pollutants at sites in this study were high in the spring due to the transboundary trans-

port of air pollutants from South Asia and Southeast Asia. Diurnal variations of air pollutants, except O₃, were characterized with bimodal peaks in the morning and later afternoon coincident with the rush hours due to the anthropogenic activities and adverse meteorological conditions, and minimum in the afternoon due to meteorological conditions good for dispersion and dilution of pollutants.

Local emissions of air pollutants in the area where the eight sites were located had a limited contribution to the high concentrations of air pollutants. SO₂ concentrations at eight sites in southwestern China were primarily affected by the air masses from central China, and O₃ concentrations were associated mainly with the air masses coming from the Tibetan Plateau. On the other hand, NO₂, CO, PM₁₀, and PM_{2.5} concentrations at these sites were affected primarily by the sources from South Asia, Southeast Asia, southwestern China and central China.

As one of the earliest analyses of air pollution in southwestern China, this study qualitatively described the contributions of air pollutants from transboundary transport to southwestern China. Due to the limited observation and inventory study, we used emis-

sion inventory in 2014 to compile the air pollutants concentrations observed in 2019 in CWT analysis, which may lead to some uncertainty in the results. Therefore, it should be highlighted that studies of transboundary transport of air pollutants in China should be strengthened as well as long term continuous measurements of air pollutants be carried out, serving as reference to assess the effectiveness of the strict pollution control in China in recent years.

CRedit authorship contribution statement

Xiufeng Yin: Conceptualization, Data curation, Writing - original draft. **Shichang Kang:** Writing - review & editing. **Maheswar Rupakheti:** Writing - review & editing. **Benjamin de Foy:** Writing - review & editing. **Ping Li:** Methodology. **Junhua Yang:** Visualization, Methodology. **Kunpeng Wu:** Software. **Qiangong Zhang:** Writing - review & editing. **Dipesh Rupakheti:** Conceptualization, Writing - review & editing.

Declaration of Competing Interest

The authors declare that they have no known competing financial interests or personal relationships that could have appeared to influence the work reported in this paper.

Acknowledgments

This study was supported by the National Natural Science Foundation of China (41907328), the Strategic Priority Research Program of Chinese Academy of Sciences, Pan-Third Pole Environment Study for a Green Silk Road (Pan-TPE) (XDA20040501), State Key Laboratory of Cryospheric Science (SKLCS-ZZ-2020). Q.G. Zhang acknowledges financial support from the Youth Innovation Promotion Association of Chinese Academy of Sciences (2016070). X.F. Yin acknowledges financial support from the Chinese Academy of Sciences "Light of West China" Program. Dipesh Rupakheti acknowledges CAS-President's International Fellowship Initiative (PIFI, Grant No. 2019PC0076). Maheswar Rupakheti acknowledges the support provided by the Institute for Advanced Sustainability Studies (IASS), which is funded by the German Federal Ministry for Education and Research (BMBF) and the Brandenburg Ministry for Science, Research and Culture (MWFK). The authors acknowledge the China National Environmental Monitoring Center and the National Oceanic and Atmospheric Administration for providing the data.

Appendix A. Supplementary data

Supplementary data to this article can be found online at <https://doi.org/10.1016/j.gsf.2021.101239>.

References

Atkinson, R., 2000. Atmospheric chemistry of VOCs and NO_x. *Atmos. Environ.* 34, 2063–2101.

Chan, C.K., Yao, X., 2008. Air pollution in mega cities in China. *Atmos. Environ.* 42 (1), 1–42.

Chen, X.L., Ma, Y.M., Kelder, H., Su, Z., Yang, K., 2011. On the behaviour of the tropopause folding events over the Tibetan Plateau. *Atmos. Chem. Phys.* 11 (10), 5113–5122.

Cheng, L., Ji, D., He, J., Li, L., Du, L.i., Cui, Y., Wang, Y., Zhang, H., Zhou, L., Li, Z., Zhou, Y., Miao, S., Gong, Z., 2019. Characteristics of air pollutants and greenhouse gases at a regional background station in southwestern China. *Aerosol. Air Qual. Res.* 19 (5), 1007–1023.

Cong, Z., Kang, S., Kawamura, K., Liu, B., Wan, X., Wang, Z., Gao, S., Fu, P., 2015. Carbonaceous aerosols on the south edge of the Tibetan Plateau: concentrations, seasonality and sources. *Atmos. Chem. Phys.* 15 (3), 1573–1584.

Draxler, R.R., Rolph, G.D., 2003. HYSPLIT (Hybrid Single-Particle Lagrangian Integrated Trajectory) Model access via NOAA ARL READY. NOAA Air Resources Laboratory, Silver Spring, MD. <http://ready.arl.noaa.gov/HYSPLIT.php>.

Duo, B., Cui, L., Wang, Z., Li, R., Zhang, L., Fu, H., Chen, J., Zhang, H., Qiong, A., 2018. Observations of atmospheric pollutants at Lhasa during 2014–2015: Pollution status and the influence of meteorological factors. *J. Environ. Sci.* 63, 28–42.

Guan, W.-J., Zheng, X.-Y., Chung, K.F., Zhong, N.-S., 2016. Impact of air pollution on the burden of chronic respiratory diseases in China: time for urgent action. *Lancet.* 388 (10054), 1939–1951.

Hsu, Y.-K., Holsen, T.M., Hopke, P.K., 2003. Comparison of hybrid receptor models to locate PCB sources in Chicago. *Atmos. Environ.* 37 (4), 545–562.

Huang, Y., Shen, H., Chen, H., Wang, R., Zhang, Y., Su, S., Chen, Y., Lin, N., Zhuo, S., Zhong, Q., Wang, X., Liu, J., Li, B., Liu, W., Tao, S., 2014. Quantification of global primary emissions of PM_{2.5}, PM₁₀, and TSP from combustion and industrial process sources. *Environ. Sci. Technol.* 48 (23), 13834–13843.

Huang, T., Zhu, X., Zhong, Q., Yun, X., Meng, W., Li, B., Ma, J., Zeng, E.Y., Tao, S., 2017. Spatial and temporal trends in global emissions of nitrogen oxides from 1960 to 2014. *Environ. Sci. Technol.* 51 (14), 7992–8000.

Kan, H., Chen, R., Tong, S., 2012. Ambient air pollution, climate change, and population health in China. *Environ. Int.* 42, 10–19.

Kang, S., Zhang, Q., Qian, Y., Ji, Z., Li, C., Cong, Z., Zhang, Y., Guo, J., Du, W., Huang, J., 2019. Linking atmospheric pollution to cryospheric change in the Third Pole Region: Current progresses and future prospects. *Natl. Sci. Rev.* 6 (4), 796–809.

Lamarque, J.-F., Emmons, L.K., Hess, P.G., Kinnison, D.E., Tilmes, S., Vitt, F., Heald, C. L., Holland, E.A., Lauritzen, P.H., Neu, J., Orlando, J.J., Rasch, P.J., Tyndall, G.K., 2012. CAM-chem: description and evaluation of interactive atmospheric chemistry in the Community Earth System Model. *Geosci. Model Dev.* 5 (2), 369–411. <https://doi.org/10.5194/gmd-5-369-2012>.

Li, C., Bosch, C., Kang, S., Andersson, A., Chen, P., Zhang, Q., Cong, Z., Chen, B., Qin, D., Gustafsson, Ö., 2016. Sources of black carbon to the Himalayan-Tibetan Plateau glaciers. *Nat. Commun.* 7, 1–7.

Lu, X., Zhang, L., Wang, X., Gao, M., Li, K., Zhang, Y., Yue, X., Zhang, Y., 2020. Rapid increases in warm-season surface ozone and resulting health impact over China since 2013. *Environ. Sci. Technol. Lett.* 7 (4), 240–247.

Luo, J., Liang, W., Xu, P., Xue, H., Zhang, M., Shang, L., Tian, H., 2019. Seasonal features and a case study of tropopause folds over the Tibetan Plateau. *Adv. Meteorol.* 2019, 1–12.

Lüthi, Z.L., Škerlak, B., Kim, S.-W., Lauer, A., Mues, A., Rupakheti, M., Kang, S., 2015. Atmospheric brown clouds reach the Tibetan Plateau by crossing the Himalayas. *Atmos. Chem. Phys.* 15 (11), 6007–6021.

Ma, Z., Xu, J., Quan, W., Zhang, Z., Lin, W., Xu, X., 2016. Significant increase of surface ozone at a rural site, north of eastern China. *Atmos. Chem. Phys.* 16 (6), 3969–3977.

Murano, K., Mukai, H., Hatakeyama, S., Suk Jang, E., Uno, I., 2000. Transboundary air pollution over remote islands in Japan: observed data and estimates from a numerical model. *Atmos. Environ.* 34 (29–30), 5139–5149.

Oh, H.-R., Ho, C.-H., Kim, J., Chen, D., Lee, S., Choi, Y.-S., Chang, L.-S., Song, C.-K., 2015. Long-range transport of air pollutants originating in China: A possible major cause of multi-day high-PM10 episodes during cold season in Seoul. *Korea. Atmos. Environ.* 109, 23–30.

Qin, Y., Xie, S.D., 2011. Historical estimation of carbonaceous aerosol emissions from biomass open burning in China for the period 1990–2005. *Environ. Pollut.* 159 (12), 3316–3323.

Qin, X., Yan, H., Zhan, Z., Li, Z., 2014. Characterising vegetative biomass burning in China using MODIS data. *Int. J. Wildland. Fire.* 23 (1), 69. <https://doi.org/10.1071/WF12163>.

Rupakheti, D., Yin, X., Rupakheti, M., Zhang, Q., Li, P., Rai, M., Kang, S., 2021. Spatio-temporal characteristics of air pollutants over Xinjiang, northwestern China. *Environ. Pollut.* 268, 115907. <https://doi.org/10.1016/j.envpol.2020.115907>.

Saikawa, E., Panday, A., Kang, S., Gautam, R., Zusman, E., Cong, Z., Somanathan, E., Adhikary, B., 2019. Air pollution in the Hindu Kush Himalaya. In: Wester, P., Mishra, A., Mukherji, A., Shrestha, A. (Eds.), *The Hindu Kush Himalaya Assessment*. Springer, Cham, pp. 339–387.

Seibert, P., Kromp-Kolb, H., Baltensperger, U., Jost, D., Schwikowski, M., Kasper, A., Puxbaum, H., 1994. In: Gryning, S.E., Millán, M.M. (Eds.), *In: Air Pollution Modeling and Its Application X*. NATO. Challenges of Modern Society, 18. Springer, pp. 689–693.

Sheng, J., Wang, X., Gong, P., Joswiak, D.R., Tian, L., Yao, T., Jones, K.C., 2013. Monsoon-driven transport of organochlorine pesticides and polychlorinated biphenyls to the Tibetan Plateau: three year atmospheric monitoring study. *Environ. Sci. Technol.* 47 (7), 3199–3208.

Shi, Y., Matsunaga, T., Yamaguchi, Y., Li, Z., Gu, X., Chen, X., 2018. Long-term trends and spatial patterns of satellite-retrieved PM_{2.5} concentrations in South and Southeast Asia from 1999 to 2014. *Sci. Total. Environ.* 615, 177–186.

Song, C., Wu, L., Xie, Y., He, J., Chen, X.i., Wang, T., Lin, Y., Jin, T., Wang, A., Liu, Y., Dai, Q., Liu, B., Wang, Y.-N., Mao, H., 2017. Air pollution in China: status and spatiotemporal variations. *Environ. Pollut.* 227, 334–347.

Tang, W., Emmons, L.K., Arellano Jr, A.F., Gaubert, B., Knote, C., Tilmes, S., Buchholz, R.R., Pfister, G.G., Diskin, G.S., Blake, D.R., Blake, N.J., Meinardi, S., DiGangi, J.P.,

- Choi, Woo, J.-H., He, C., Schroeder, J.R., Suh, I., Lee, H.-J., Jo, H.-Y., Kanaya, Y., Jung, J., Lee, Y., Kim, D., . Source contributions to carbon monoxide concentrations during KORUS-AQ based on CAM-chem model applications. *J. Geophys. Res. Atmos.* 124 (5), 2796–2822.
- Verstraeten, W.W., Neu, J.L., Williams, J.E., Bowman, K.W., Worden, J.R., Boersma, K. F., 2015. Rapid increases in tropospheric ozone production and export from China. *Nat. Geosci.* 8 (9), 690–695.
- Wang, Y.Q., Zhang, X.Y., Draxler, R.R., 2009. TrajStat: GIS-based software that uses various trajectory statistical analysis methods to identify potential sources from long-term air pollution measurement data. *Environ. Model. Softw.* 24 (8), 938–939.
- Wang, S., Hao, J., 2012. Air quality management in China: Issues, challenges, and options. *J. Environ. Sci.* 24 (1), 2–13.
- Wang, Y.Q., 2014. Meteoinfo: GIS software for meteorological data visualization and analysis. *Meteorol. Appl.* 21 (2), 360–368.
- Wang, Y., Ying, Q., Hu, J., Zhang, H., 2014. Spatial and temporal variations of six criteria air pollutants in 31 provincial capital cities in China during 2013–2014. *Environ. Int.* 73, 413–422.
- Wang, Y., Zhang, Y., Schauer, J.J., de Foy, B., Guo, B., Zhang, Y., 2016. Relative impact of emissions controls and meteorology on air pollution mitigation associated with the Asia-Pacific Economic Cooperation (APEC) conference in Beijing, China. *Sci. Total. Environ.* 571, 1467–1476.
- Yang, J., Ji, Z., Kang, S., Zhang, Q., Chen, X., Lee, S.-Y., 2019. Spatiotemporal variations of air pollutants in western China and their relationship to meteorological factors and emission sources. *Environ. Pollut.* 254, 112952. <https://doi.org/10.1016/j.envpol.2019.07.120>.
- Yin, D., Zhao, S., Qu, J., 2017. Spatial and seasonal variations of gaseous and particulate matter pollutants in 31 provincial capital cities. *China. Air. Qual. Atmos. Health.* 10 (3), 359–370.
- Yin, X., Kang, S., Foy, B.D., Ma, Y., Tong, Y., Zhang, W., Wang, X., Zhang, G., Zhang, Q., 2018. Multi-year monitoring of atmospheric total gaseous mercury at a remote high-altitude site (Nam Co, 4730 m asl) in the inland Tibetan Plateau region. *Atmos. Chem. Phys.* 18, 10557–10574.
- Yin, X., de Foy, B., Wu, K., Feng, C., Kang, S., Zhang, Q., 2019. Gaseous and particulate pollutants in Lhasa, Tibet during 2013–2017: Spatial variability, temporal variations and implications. *Environ. Pollut.* 253, 68–77.
- Yin, X., Zhou, W., Kang, S., de Foy, B., Yu, Y., Xie, J., Sun, S., Wu, K., Zhang, Q., 2020. Latest observations of total gaseous mercury in a megacity (Lanzhou) in northwest China. *Sci. Total. Environ.* 720, 137494. <https://doi.org/10.1016/j.scitotenv.2020.137494>.
- Zhang, Q., He, K., Huo, H., 2012. Cleaning China's air. *Nature* 484 (7393), 161–162.
- Zhang, Q., Jiang, X., Tong, D., Davis, S.J., Zhao, H., Geng, G., Feng, T., Zheng, B., Lu, Z., Streets, D.G., Ni, R., Brauer, M., van Donkelaar, A., Martin, R.V., Huo, H., Liu, Z., Pan, D., Kan, H., Yan, Y., Lin, J., He, K., Guan, D., 2017. Transboundary health impacts of transported global air pollution and international trade. *Nature* 543 (7647), 705–709.
- Zhao, S., Yu, Y., Yin, D., He, J., Liu, N., Qu, J., Xiao, J., 2016. Annual and diurnal variations of gaseous and particulate pollutants in 31 provincial capital cities based on in situ air quality monitoring data from China National Environmental Monitoring Center. *Environ. Int.* 86, 92–106.
- Zhao, S., Yu, Y., Qin, D., 2018. From highly polluted inland city of China to "Lanzhou Blue": The air-pollution characteristics. *Sci. Cold. Arid. Reg.* 10, 12–26.
- Zhong, Q., Huang, Y., Shen, H., Chen, Y., Chen, H., Huang, T., Zeng, E.Y., Tao, S., 2017. Global estimates of carbon monoxide emissions from 1960 to 2013. *Environ. Sci. Pollut. R.* 24 (1), 864–873.